

Polaron Plasma in Equilibrium with Bright Excitons in 2D and 3D Hybrid Perovskites

Angelica Simbula, Riccardo Pau, Qingqian Wang, Fang Liu, Valerio Sarritzu, Stefano Lai, Matteo Lodde, Francesco Mattana, Guido Mula, Alessandra Geddo Lehmann, Ioannis D. Spanopoulos, Mercouri G. Kanatzidis, Daniela Marongiu, Francesco Quochi, Michele Saba,* Andrea Mura, and Giovanni Bongiovanni

Rapid advances in perovskite photovoltaics have produced efficient solar cells, with stability and duration improving thanks to variations in materials composition, including the use of layered 2D perovskites. A major reason for the success of perovskite photovoltaics is the presence of free carriers as majority optical excitations in 3D materials at room temperature. On the other hand, the current understanding is that in 2D perovskites or at cryogenic temperatures insulating bound excitons form, which need to be split in solar cells and are not beneficial to photoconversion. Here, a tandem spectroscopy technique that combines ultrafast photoluminescence and differential transmission is applied to demonstrate a plasma of unbound charge carriers in chemical equilibrium with a minority phase of light-emitting excitons, even in 2D perovskites and at cryogenic temperatures. The underlying photophysics is interpreted as formation of large polarons, charge carriers coupled to lattice deformations, in place of excitons. A conductive polaron plasma foresees novel mechanisms for LEDs and lasers, as well as a prominent role for 2D perovskites in photovoltaics.

spectrum featuring a marked excitonic resonance, the majority optical excitation in prototypical HP materials for photovoltaics are not bound excitons, but unbound charge carriers. Therefore, electrons and holes excited by solar light can be directed to the electrodes at a negligible energy cost, without the need to split tightly bound excitons as in organics. Taking advantage of the flexibility of the materials class, layered 2D HPs are obtained by inserting bulky organic cations into the formulation, leading to materials inherently more stable than their 3D counterparts against degradation.^[8–10] However, in 2D HPs the exciton binding energy can be as large as 400 meV,^[8] so that it is commonly assumed that their excited states are mostly excitons.

A second peculiar characteristic of the excited states in perovskites is the formation of large polarons, that is, charge carriers coupled to lattice deformations and delocalized over many crystal lattice sites.^[11–20]

Unlike small polarons in organics, localized in a single molecule, large polarons are compatible with band transport, but are also able to screen the excited states from scattering with defects and reduce non-radiative recombination through trap states, resulting in large mobilities and long lifetimes. Large polarons are also believed to reduce scattering with phonons and have been proposed as an explanation for hot carriers persisting for several nanoseconds at temperatures significantly higher than the lattice one.^[12,16,17,21–26] Large polarons may therefore be the enabling microscopic mechanism for efficient solar cells, including innovative architectures that exploit photoconversion with hot carriers.^[27,28]


Theoretical estimations forecast that the energy associated with polaron formation is comparable with the binding energy gained by forming an exciton, maybe even larger in some materials.^[12,14,24,29–32] When do polarons form and whether excitons or polarons are the lowest-energy optical excitations is still an open question. The issue is particularly relevant for layered 2D HPs, where polaronic effects have been demonstrated, although it is not clear if small or large polarons are formed.^[33–37] In spite of the large exciton binding energy, unbound charge carriers have been reported, so that it is not clear yet how much energy needs to be spent in solar cells to split bound excitons.^[38–43]

1. Introduction

Thanks to hybrid metal-halide perovskites (HPs), solution-process materials may now be employed in efficient single-junction and tandem solar cells. Photoconversion performances in these materials have been linked to unique photophysics properties.^[1–7] First it was realized that, in spite of an absorption

Dr. A. Simbula, R. Pau, Dr. Q. Wang, F. Liu, Dr. V. Sarritzu, S. Lai, M. Lodde, F. Mattana, Dr. G. Mula, Dr. A. Geddo Lehmann, Dr. D. Marongiu, Prof. F. Quochi, Prof. M. Saba, Prof. A. Mura, Prof. G. Bongiovanni
Dipartimento di Fisica
Università di Cagliari
Monserrato I-09042, Italy
E-mail: saba@unica.it

Prof. I. D. Spanopoulos, Prof. M. G. Kanatzidis
Department of Chemistry
Northwestern University
Evanston, IL 60208, USA

 The ORCID identification number(s) for the author(s) of this article can be found under <https://doi.org/10.1002/adom.202100295>.

© 2021 The Authors. Advanced Optical Materials published by Wiley-VCH GmbH. This is an open access article under the terms of the Creative Commons Attribution License, which permits use, distribution and reproduction in any medium, provided the original work is properly cited.

DOI: 10.1002/adom.202100295

Here we present ultrafast tandem spectroscopy experiments to investigate the roles of excitons, free charged carriers, and polarons in HPs. The body of experimental results is consistent with a picture in which a majority of charged carriers, polarons, coexists with a minority of bound excitons in both 3D and 2D HPs, even when the exciton binding energy by far exceeds thermal energy.

2. Results

2.1. Ultrafast Tandem Spectroscopy

The optical properties of hybrid perovskites are typically studied with two ultrafast spectroscopy techniques, namely time-resolved photoluminescence (PL) and differential transmission (DT), also known as transient absorption or pump-probe. The two techniques probe different properties and are complementary to each other. PL is only sensitive to radiative species, as it collects the light emitted from the sample under pulsed laser excitation. On the other hand, DT is sensitive to all optical excitations, even if they cannot emit light (“dark states”), since a DT signal may arise from phase space filling in only one of the two bands involved (conduction or valence), but also from collisional broadening and other nonlinear interactions that do not require the same states to be occupied (see Figure S1, Supporting Information). Therefore, a DT signal can be produced even by excitations that are completely dark in PL. Furthermore, the DT signal is directly proportional to the excited-state population density, while the PL signal follows a power law with

an exponent equal to the order of the recombination process leading to the emission: it is directly proportional to population density for monomolecular recombination, while proportional to the square of the population for bimolecular recombination. The synergy between the two techniques should therefore yield information on the nature of majority photoexcitations and whether or not they emit light. A previous study^[44] has linked the two measurements on MAPbI₃ films employed for solar cells. A crucial experimental hurdle for quantitative comparison of PL and DT is that the time decays are inherently non-linear in the excitation density, that is, they change with laser fluence. Furthermore, different spots on a thin film surface may produce different decay times. DT and PL setups may employ excitation laser pulses with different duration, different wavelength, and may be focused to a different waist, leading to different spatial excitation profiles and time decays that are not easily comparable.

We solved this issue by combining the two measurements into a single ultrafast tandem spectroscopy setup (see **Figure 1**): femtosecond laser pulses excite the sample and PL emission is detected by a picosecond streak camera, while, in the same setting, a transient change in the absorption coefficient is probed by delayed weak broadband laser pulses dispersed in a differential spectrometer. By construction, both PL and DT are produced with the very same train of laser pulses, creating the same excitation density; as shown in Figure 1, the two signals are collected from two largely overlapping sample spots.

We then set to apply the tandem spectroscopy technique to understand the relationship between excitons, polarons, and free carriers in 2D and 3D HPs. Materials were selected

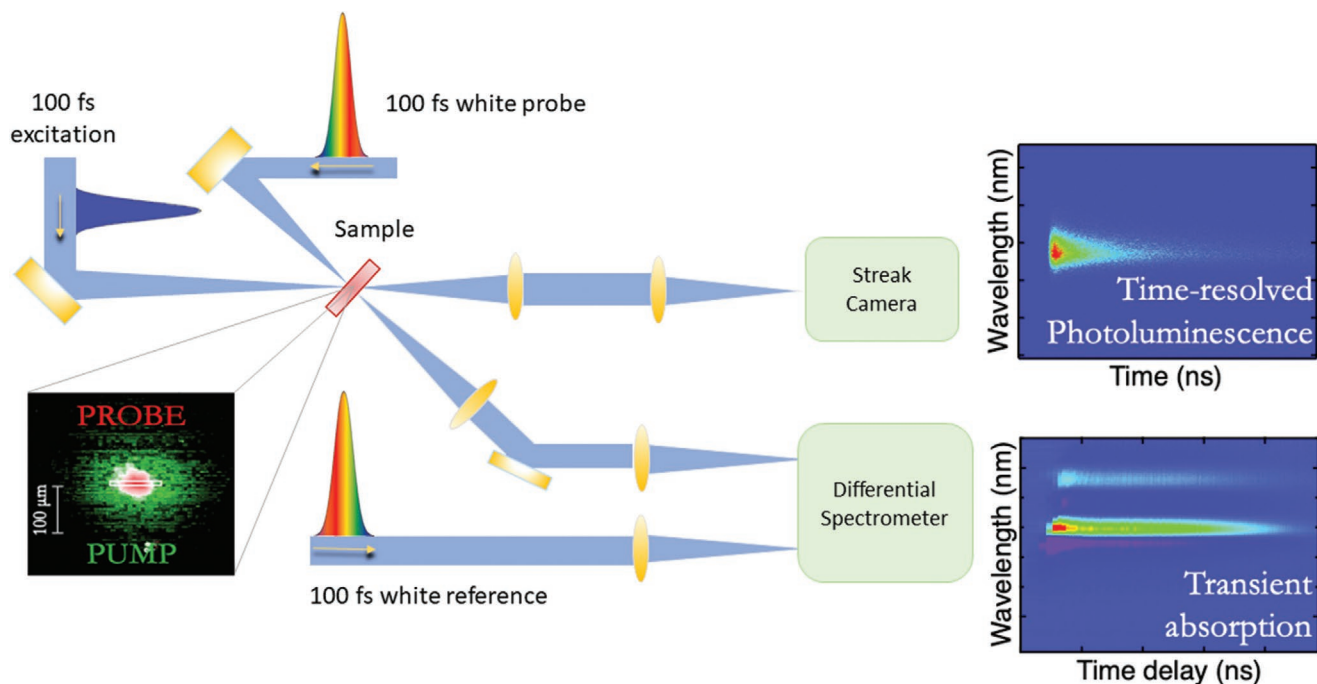


Figure 1. Ultrafast tandem spectroscopy setup. The sketch illustrates how a femtosecond pump laser is focused onto samples and then time-resolved PL is detected with a picosecond streak camera, while a second broadband femtosecond pulse acts as a probe for DT. The crucial feature of the setup is that the same pump pulses cause the two effects, which therefore occur by construction at the same excitation density and spot on the sample. In the lower left corner are shown the superimposed images of the probe spot, on which DT is measured, and pump spot, with the white rectangle delimiting the area selected for PL measurements by the vertical and horizontal slits in the streak camera setup.

to represent the variety of HPs of current interest. MAPbI₃ (with MA = CH₃NH₃, methylammonium) was chosen as prototypical 3D HP absorber for single-junction solar cells, in particular we have also investigated the mixed-cation, mixed-halide variant MA_{1-x-y}FA_xCs_yPbI_{3-z}Br_z (with FA = HC(NH₂)₂, and formamidinium) where *x*, *y*, and *z* represent small fractions with respect to unity, that is successfully applied in solar cells. MAPbBr₃ has been included for its potential as light emitter in LEDs and lasers, as photon absorber in photo-detectors or as top junction semiconductor in tandem solar cells. We selected BA₂PbI₄ (BA = C₄H₁₂N, *n*-butylammonium) and BA₂SnI₄ as archetypes of Ruddlesden–Popper 2D layered HPs.^[8] Sn-based HPs were included, as replacing poisonous lead is considered a priority and such materials are currently employed to realize the highest photoconversion performances among lead-free HPs.^[45–47] The crystal structures and optical properties of the investigated HPs are shown in Figure 2 (X-ray diffraction

spectra are shown in Figure S2, Supporting Information). The onset of optical absorption spans the visible and near-infrared spectrum, ranging from 530 nm in wavelength for BA₂PbI₄ to 780 nm for MAPbI₃. The substitution of iodine with the lighter bromine halogen, as well as quantum confinement of the electronic excitations, widens the gap. The blue shift is accompanied by strengthening of the excitonic resonance at the band-edge. The increasing exciton oscillator strength is related to the larger exciton binding energy *E*_b, which happens to be comparable to room-temperature thermal energy *k*_B*T* ≅ 26 meV in MAPbI₃, but increases to 60 meV in MAPbBr₃, that is, much larger than *k*_B*T* at both *T* = 77 K and *T* = 300 K.^[48–50] In 2D HPs, excitons are very robust electronic excitations with several hundreds of meV of binding energy, depending on layer thickness, namely 10–20 times *k*_B*T* at room temperature, because of the combined effect of spatial and dielectric confinement.

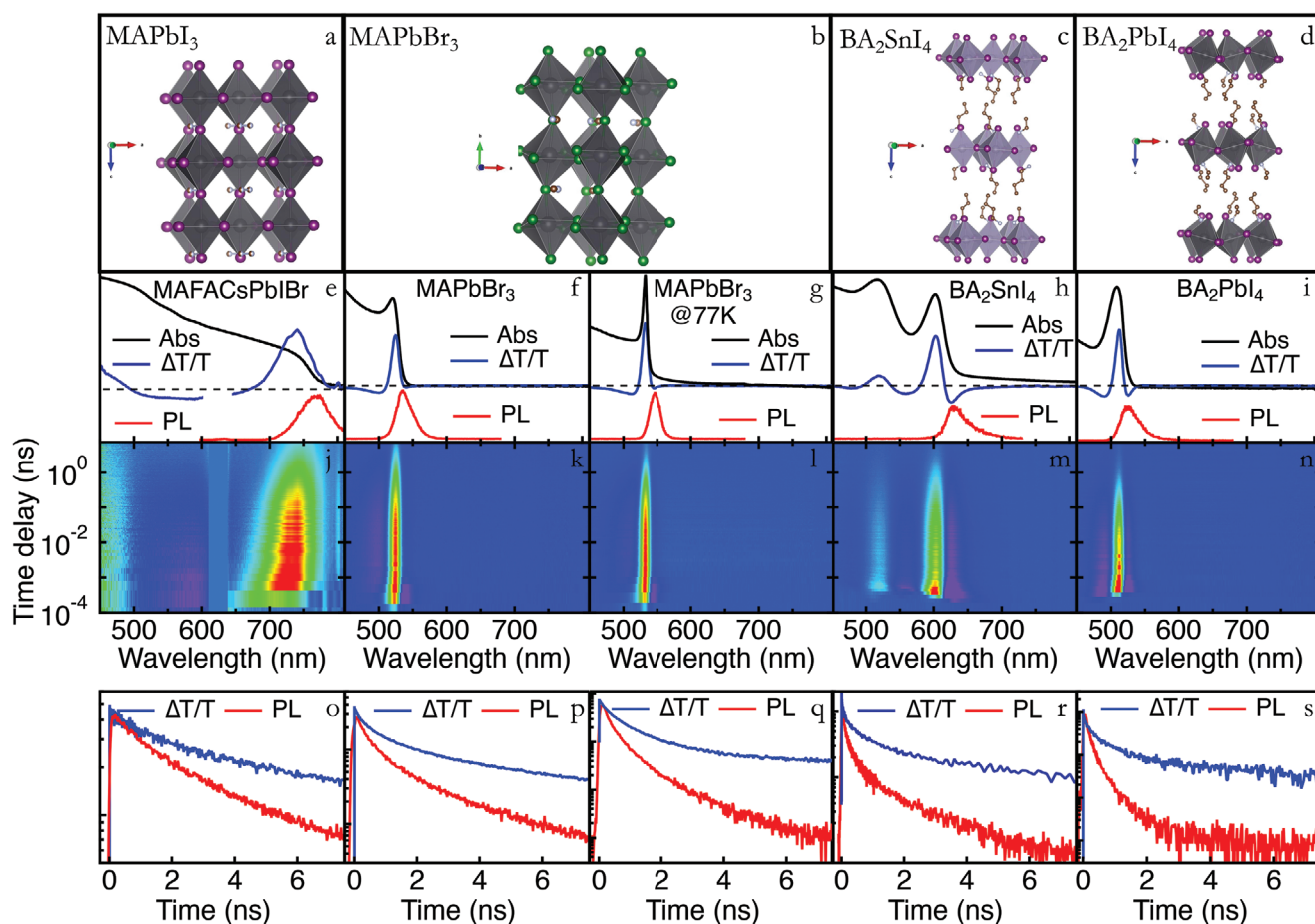


Figure 2. Ultrafast tandem spectroscopy on perovskite materials. a–d) Sketches of the crystal structure of the investigated perovskite materials are depicted in the top row, with prototypical 3D materials (MAPbI₃ and MAPbBr₃) as well as prototypical layered structures with *n* = 1 (BA₂PbI₄ and BA₂SnI₄); purple dots represent iodine atoms, green dots are bromine one; metal atoms (Pb and Sn) are shown as gray dots; only bulky butylammonium cations are shown while smaller methylammonium ones are omitted for clarity. e–i) The second row shows for each film the continuous-wave UV–vis absorption spectrum (black line), the time-integrated differential transmission spectrum (blue line) with a bleaching spectrum resonant with the exciton absorption peak, and the time-integrated photoluminescence spectrum (red line), also peaked at the exciton resonance; the MAPbBr₃ sample has been measured both at room and cryogenic temperature (77 K). The excitation wavelength was 430 nm for all samples, except for MA_{1-x-y}FA_xCs_yPbI_{3-z}Br_z, where 630 nm was employed. j–n) In the third row the complete differential transmission spectrograms are shown, with a logarithmic time axis. o–s) The fourth row depicts the comparison between the differential transmission (blue line) and photoluminescence (red line) time decays, demonstrating the photoluminescence in all samples is significantly faster than differential transmission.

All HPs we have investigated are bright light emitters. The PL spectra shown in Figure 2 are peaked on the low-energy side of the exciton absorption transition. The reciprocity law between absorption and emission forecasts the correct emission spectrum by simply multiplying the absorptance spectrum by the Boltzmann factor to account for population decreasing with increasing energy, as shown in Figure S3, Supporting Information. Reciprocity, therefore, demonstrates that light is emitted by the same states responsible for band-edge absorption, a feature widely accepted in literature and even employed to correlate the emission quantum yield with photovoltaic performance.^[7,51–53] In HPs with exciton binding energy much larger than thermal energy, $E_b \gg k_B T$, such as the layered 2D HPs, or MAPbBr₃ at low temperature, such reciprocity relation implies that emission is excitonic in nature, because free-carrier emission would be peaked in spectrum at higher photon energies, blueshifted by $\cong E_b$ with respect to exciton emission, well outside the linewidth of the observed PL spectrum. MAPbI₃ and MA_{1-x-y}FA_xCs_yPbI_{3-z}Br_z represent a borderline situation, since $E_b \cong k_B T$ and thus the intensity of light emission from free electron-hole pairs may become comparable to the exciton emission, especially at the high-energy side of the PL spectrum. Whenever free carriers are majority optical excitations however, the emission dynamics turns out to be independent of the nature of the emitting species, free carriers or excitons, since a bimolecular process is always involved, whether is exciton formation as intermediate step before emission or direct recombination of free carriers.

The DT signal in all HPs shows a dominant bleaching feature, resonant with the lowest excitonic transition, with photoinduced absorption sidebands due to many-body effects.^[6,11,54–56] The DT spectrum does not change with the delay, apart from the ultrafast spectral dynamics observed in the first 2ps after excitation, which will be discussed later. The PL decays and the DT transients measured under the same conditions in a window of several nanoseconds after excitation (extracted in a spectral window around the bleaching peak) are compared in Figure 2o–s. The comparison between the two transients provides the main preliminary information: PL decays are much faster than the corresponding DT ones, in all HPs. If we assume that the DT signal probes the time evolution of the majority photoexcitations, regardless of whether they are excitons or charged carriers, DT and PL signals are expected to be proportional to each other if the majority species are excitons, emitting light through a monomolecular process. The experimental evidence suggests instead that the majority photoexcited species are charged carriers, requiring a bimolecular process to recombine and therefore causing the PL signal to be proportional to the square of the excited population and to decay faster than DT. While such a picture is familiar for MAPbI₃ and MAPbBr₃ at room temperature, it is very surprising that the PL intensity decays faster than DT also for MAPbBr₃ at 77 K and even for 2D HPs in which $E_b \gg k_B T$ and majority excitons are expected for all available photoexcitation densities. The possibility that the DT signal could be induced by a minority population of free carriers in a sea of majority excitons can be ruled out on the basis of the expected and observed scaling laws of the PL and DT signals on the laser pulse fluence. If the DT were induced by minority phase of charged carriers, the

$PL(t = 0) \cong PL_0$ intensity would scale linearly with the majority exciton population and thus with the laser fluence, while the DT signal would not be expected to increase linearly, in contrast with experimental observations shown in the insets of Figure 3. The tandem spectroscopy results demonstrate therefore that excitons are always a minority species and are immersed in a plasma of unbound charge carriers. Clearly excitons are still formed, since PL is emitted from excitons, consistently with recent reports,^[38–42] but they are not the majority species.

2.2. Bimolecular Photoluminescence and Minority Excitons

To study the extent to which photon emission in HPs stems from bimolecular recombination of charged carriers, we quantitatively compare the PL and DT transients, the latter being proportional to the photoexcitation population. Accordingly, Figure 3 reports the PL decays as a function of the laser pulse fluence Φ together with the square of the corresponding DT traces, namely $\left(\frac{\Delta T}{T}\right)^2$, rescaled to match the PL transients.

In 3D HPs, PL and DT squared traces are remarkably superimposed. Deviations from this behaviour are only observed at low temperature and for long delay times in MAPbBr₃. In 2D BASnI₄, the superpositions of the two signals are satisfactory at all densities. A transient overshooting of the PL signal is, however, detected at short delays and lower laser fluences. This behavior was also recorded in 2D BAPbI₄ together with a slower decay of the DT signal at long times for the highest excitation rates. A good agreement between PL and DT squared traces may only occur if PL is generated through bimolecular recombination from the reservoir of photoexcitations that causes the DT signal. Two are the possible scenarios compatible with such dynamics: either free carriers recombine directly to emit light, or excitons are formed in equilibrium as a minority species through bimolecular pairing of free carriers and then emit light with a monomolecular process. The second scenario, exciton emission, appears as the one compatible with reciprocity in 2D HPs and in MAPbBr₃ at low temperature, given the fact that the optical emission spectrum is resonant with excitonic absorption. We will therefore adopt from now on the picture of minority bright excitons immersed in a majority plasma of free carriers, since it is the only one compatible with the entire body of experimental data. Possible explanations for the variance from the PL $\left(\frac{\Delta T}{T}\right)^2$ behaviour will be discussed later on.

The equilibrium condition for excitons and free carriers is predicted by Saha equation,^[2,4–6] in the form $n_{cc}^2(t) = n_{eq} n_x(t)$, where $n_x(t)$ and $n_{cc}(t)$ are the population densities of excitons and charged carriers at time t , while n_{eq} is the equilibrium constant. Since charge carriers are the majority population, $n_{cc} \gg n_x$, then $\frac{\Delta T}{T}(t) \propto n_{cc}(t)$, while $PL(t) \propto n_x(t)$, so that the equilibrium condition implies that $PL \propto \left(\frac{\Delta T}{T}\right)^2$, in agreement with experimental results. The kinetics of the two photoexcitations can therefore be described as a time-sequence of chemical equilibrium states in which the population of one species determines the population of the other one. As a consequence, whatever annihilation process the two types of photoexcitations

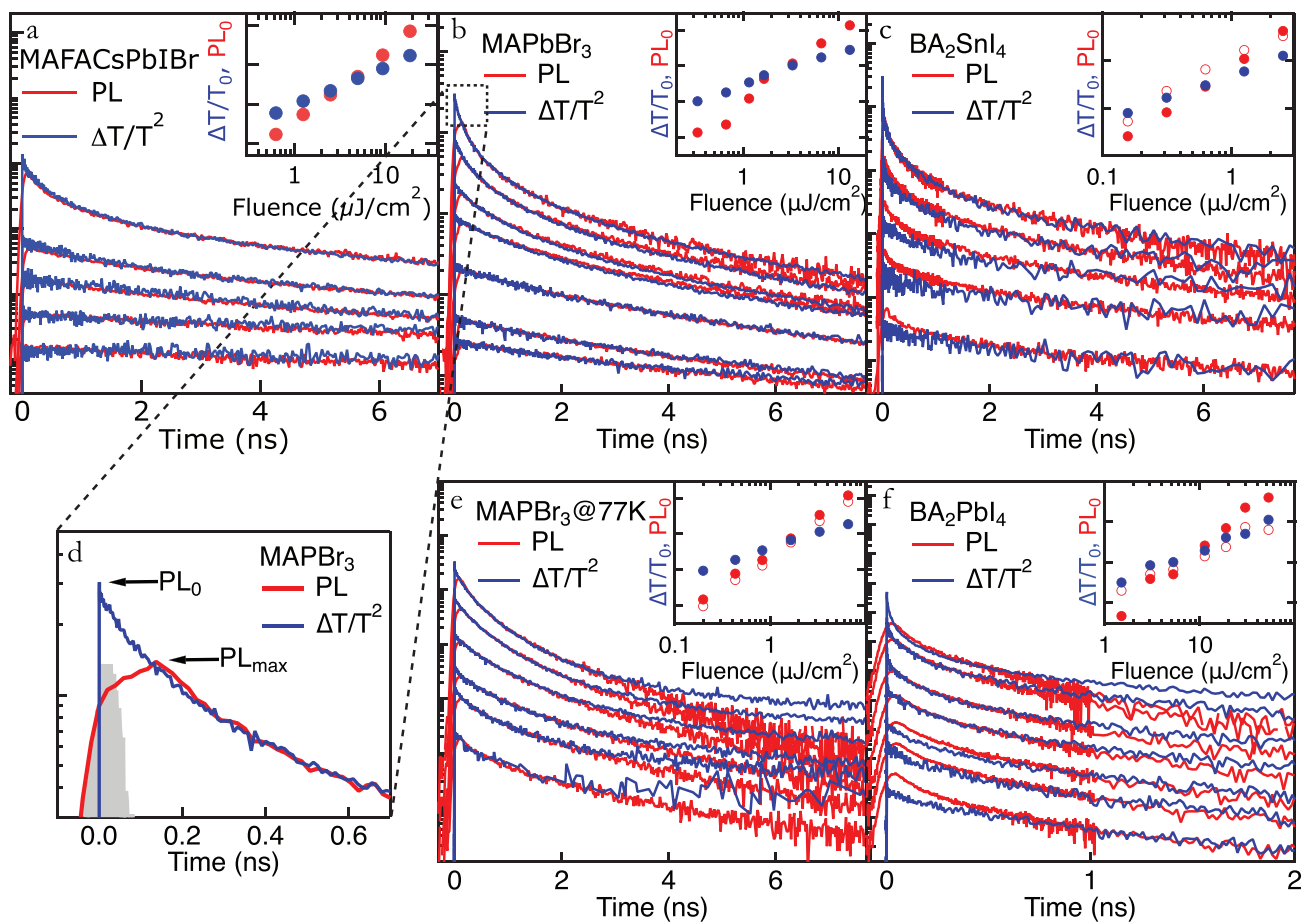


Figure 3. Comparison between photoluminescence and square of differential transmission. Panels a–c) and e,f) show for each sample the photoluminescence decays (red lines) and the square of differential transmission decays (blue lines, extracted at the maximum of the bleaching signal) as a function of laser fluence. Each pair of decays is measured with the same fluence. The close correspondence between photoluminescence and the square of differential transmission demonstrates that the two techniques monitor two different species, excitons and charged carriers, respectively, in chemical equilibrium. The inset in each panel shows as a function of laser fluence the power law for the initial values of differential transmission (solid blue dots), which happens to be linear, and photoluminescence (solid red dots), which instead is quadratic. The temporal resolution of the streak camera smoothens the initial photoluminescence transient; to compensate for such an effect, the initial value for the photoluminescence is extracted from the square of the corresponding differential transmission decay, where temporal resolution is around 100 fs. Panel (d) illustrates the difference between the correct value PL_0 extrapolated according to the procedure and the maximum intensity PL_{max} (maximum values are also added in some insets as empty red dots to visually demonstrate how the apparent power law for PL can be affected by the limited resolution). The curve delimiting the gray-colored area represents the streak camera response function, that is, the temporal resolution of the detection apparatus.

undergo, the interconversion rate between bound and unbound pairs is always fast enough to guarantee the thermodynamic equilibrium. Significant effects from non-thermal or hot carrier populations were excluded (see Figure S4, Supporting Information).

The equilibrium condition is further supported by the quadratic dependence of the $PL(t=0) \equiv PL_0$ intensity on the pulse fluence and the $\frac{\Delta T}{T}(t=0) \equiv \frac{\Delta T}{T}|_0$ linear dependence, as shown in the inset of the MAPbBr₃ panel of Figure 3. At the highest excitations, the initial transient of the exciton population is very fast and cannot be correctly captured by our PL streak-camera apparatus due to its 50-ps time resolution. The method used to extrapolate PL_0 for kinetics faster than the experimental resolution time is illustrated in the lower-left panel of Figure 3. Even when PL results from radiative annihilation of

excitons through a monomolecular process, the exciton density increases quadratically with the overall photoexcitation population as long as charged carriers are the majority species and the quasi-stationary Saha equilibrium is achieved. The super-linear PL dependence on the DT signals, close to a quadratic power-law in all HPs, appears as a general, intrinsic feature of 3D and 2D perovskite photophysics and does not depend on extrinsic factors such as traps and defects; results shown in Figure 3 were replicated (see Figure S5, Supporting Information) for a pure MAPbI₃ perovskite, even though the PL lifetime at low fluences was significantly shorter. Moreover, a quadratic PL with respect to injected carrier concentration was observed even under resonant excitation at the exciton peak in MAPbBr₃ at cryogenic temperatures, both under one photon and two-photon excitation (Figure S6, Supporting Information).

The Saha equation forecasts that the ratio of excitons to free carriers increases with excitation fluence so that, for excited-state densities above the equilibrium constant $n_{\text{eq}} = \left(\frac{k_B T \tilde{m}_{\text{eh}}}{2\pi\hbar^2}\right)^3 e^{-\frac{E_b}{k_B T}}$ most of the photoexcitations are excitons (\tilde{m}_{eh} is the reduced electron–hole mass). For MAPbI₃, $E_b \cong 26$ meV and therefore the equilibrium density is $n_{\text{eq}} \cong 1.5 \times 10^{17} \text{ cm}^{-3}$. In MAPbBr₃ ($E_b = 64$ meV) the predicted crossover occurs at $n_{\text{eq}} \cong 3.3 \times 10^{16} \text{ cm}^{-3}$ for $T = 300$ K and $n_{\text{eq}} \cong 3.3 \times 10^{12} \text{ cm}^{-3}$ for $T = 77$ K. Above such densities, both PL and DT should monitor the exciton population, and thus $PL \propto \frac{\Delta T}{T}$ is predicted by Saha equilibrium. In all 3D HPs, the densities of photoexcitations created by laser pulses range from slightly above 10^{16} cm^{-3} to more than 10^{18} cm^{-3} (see Table S1, Supporting Information), therefore largely exceeding n_{eq} by several orders of magnitude at low temperature. Yet, all experimental results reported in Figure 3 show $PL \propto \left(\frac{\Delta T}{T}\right)^2$, meaning that the crossover to an exciton majority was never observed. One possible explanation could be a decrease in E_b for increasing excitation, owing to many-body effects. Yet, this interpretation is ruled out by the observation of a still intense exciton resonance in absorption even at the highest excitation regimes investigated in our experiments (see Figure S7, Supporting Information). Since the exciton oscillator strength f is related to the binding energy by $f \propto E_b^{1.5}$, a marginal reduction in the exciton oscillator strength, for example, by ten percent, implies that E_b is not significantly reduced either.

The most surprising result in Figure 3 is that the linear relationship, $PL \propto \frac{\Delta T}{T}$, was never observed even in 2D HPs, in spite of their giant exciton binding energies. Saha crossover density in two dimensions reads $n_{\text{eq}}^{2D} = \frac{\tilde{m}_{\text{eh}} k_B T}{2\pi\hbar^2} e^{-\frac{E_b}{k_B T}} \cong 5 \times 10^6 \text{ cm}^{-2}$ for $E_b \cong 300$ meV at room temperature. In the density regime we explored, $10^9 - 10^{12} \text{ cm}^{-2}$ (see Table S1, Supporting Information), virtually all photoexcitations are predicted to be excitons, the opposite of what is observed.

3. Discussion

3.1. Polaron Plasma

The formation of a charged carrier plasma as majority photoexcitation at all excitation regimes and in all HP materials calls for a fundamental physical mechanism that favors accumulation of a high density of unbound electrons and holes with respect to bound and charge-neutral excitons. The one mechanism up to now neglected in our analysis is carrier-lattice interaction, which can induce the formation of large charged polarons, as well documented in literature.^[11–20] Dressing charged carriers by lattice deformations brings two main consequences: the first one is that polarons are energetically stabilized with respect to free electrons and holes, meaning that they sit at lower energy and therefore effectively reduce the exciton binding energy; the second one is the heavier mass of polarons

than free carriers, which increases the density of states making them entropically favored with respect to excitons. Both effects reduce the probability of exciton formation, as also inferred from the analytical expression of the modified Saha constant

$n_{\text{eq}} = \left(\frac{k_B T \tilde{m}_p}{2\pi\hbar^2}\right)^3 e^{-\frac{E_b - (E_{p+} + E_{p-})}{k_B T}}$, in which the exciton binding energy E_b is reduced by the stabilization energy for the two polarons ($E_{p+} + E_{p-}$), and \tilde{m}_{eh} is replaced by the much larger mass $\tilde{m}_p = \frac{m_{p+} m_{p-}}{m_e + m_h}$, where m_{p+} , m_{p-} and $m_{e,h}$ are the polaron and free carrier masses, respectively (see Experimental Section for derivation).

We now focus on the situations when experimental data reported in Figure 3 deviate from the behavior $PL \propto \left(\frac{\Delta T}{T}\right)^2$, meaning that the equilibrium condition is not met. We first examine the decay of $\left(\frac{\Delta T}{T}\right)^2$ in MAPbBr₃ at 77 K, which becomes slower than the PL's one at long times after excitation. Similar deviations are also observed in BA₂PbI₄. We attribute such deviations to unbalanced populations of positive (n_{p+}) and negative (n_{p-}) polarons that occur at low concentrations due to a more efficient trapping of one of the two polarons by deep defects (or preferential formation of small polarons of one type). Since $PL \propto n_X \propto (n_{p+} \times n_{p-})$, while $\frac{\Delta T}{T} \propto (n_{p+} + n_{p-})$, unbalanced polaron populations ($n_{p+} \neq n_{p-}$) cause the PL signal to decay faster than the square of DT ($PL < \left(\frac{\Delta T}{T}\right)^2$) once the two signals have been normalized at $t = 0$). Tandem spectroscopy proves therefore a suitable optical tool to single out contribution from traps and defects, a key issue in this class of materials.^[57]

The deviations from equilibrium observed at short times in 2D HPs, both BA₂SnI₄ and BA₂PbI₄, seem instead of intrinsic nature and could represent the transient photoexcitation dynamics preceding the establishing of chemical equilibrium between excitons and polarons. The $\left(\frac{\Delta T}{T}\right)^2$ curves have been rescaled to fit the long-time PL decays, when light emission results from the excitonic population in equilibrium with polarons. The PL signal at early times overshoots the DT squared one, especially for low fluences. Such overshoot is rationalized as originating from emission of out-of-equilibrium, geminate excitons, directly created in the absorption process, which dissociate into unbound polaron pairs a few hundred picoseconds after generation. While barely visible for 3D HPs, the observation of geminate excitons becomes evident in 2D systems, presumably due to the stronger Coulomb attraction between photogenerated charged pairs.^[58] The finite PL time resolution at the highest fluences in combination with the geminate emission at the lowest excitations explains why the power-law dependence of PL_0 on fluence Φ leads to an exponent smaller than two, as also recently reported.^[59] We finally mention that the stronger contribution of geminate excitons at lower fluences may imply that thermodynamic equilibrium is not fully established at the carrier generation rates typically involved under continuous-wave excitations, as, for example, those achievable under solar illumination or LEDs.

3.2. Markov Dynamics, Rate Equations, and Identification of Decay Processes

Polarons and excitons decay through different channels, so that both their population densities are needed to reproduce the observed dynamics. The equilibrium condition however locks the PL and DT decays to each other, since the ratio between the concentration of polarons, n_p (assuming $n_{p+} = n_{p-}$), and excitons, n_x , is fully determined by the equilibrium condition $n_p^2 = n_{eq} n_x$. As a result, the recombination rates of the photo-excited carriers only depend on the instantaneous value of the total excited-state density $n = n_p + n_x \cong n_p$, regardless of the previous history of the photoexcitations, a situation often referred to as a Markovian process. To highlight the Markov dynamics, DT and PL traces measured for different initial densities can be shifted on the horizontal time axis so that they overlap;^[60] the decays obtained for lower fluences match the tails of the ones obtained for higher fluences, as they refer to the same excited-state density. **Figure 4** demonstrates such a property for both DT and PL decays in all the HPs we have studied. PL and DT traces measured for the same fluence were obviously shifted by the same delay.

While the experimental results clearly show the Markovian nature of the decay of polarons and excitons, few deviations are noticeable in films where trapping of just one type of polarons occurs. In these regimes, the fate of the photoexcitations also depends on the preceding history, namely on the density of long lived trapped polarons. The contribution of

non-equilibrium geminate excitons to the PL signal does not satisfy either, as expected, the Markovian test, since the time-shifted decays deviate from a universal curve. Concerning the ubiquitous sub-picosecond spike observed in DT decay curves reported in Figure 4, and widely reported in literature, its analysis, detailed in the Experimental Section, is consistent with the ultrafast polaron formation dynamics and highlights the involved many-body effects.

We have now all the elements to identify and quantify the decay processes through the population rate equations, which should account for the main findings emerged from tandem spectroscopy: the chemical equilibrium between excitons and polarons, the prevalence of the polaron population, and the Markovian nature of the recombination processes. As shown in the Experimental Section, these conditions lead to the following rate equations for the populations of the majority (polarons, n_p) and minority (excitons, n_x) species:

$$\dot{n}_p \cong -k_{1,p}n_p - \left(k_{r,p} + \frac{k_{1,x}}{n_{eq}}\right)n_p^2 - k_{3,p}n_p^3 \quad (1)$$

$$\dot{n}_x \cong -2k_{1,p}n_x - 2\left(k_{r,p} + \frac{k_{1,x}}{n_{eq}}\right)\frac{1}{2}n_{eq}^{\frac{1}{2}}n_x^{\frac{3}{2}} - 2k_{3,p}n_{eq}n_x^2 \quad (2)$$

Equation (1) holds for both positively and negatively charged polarons, as their populations, created equal by photoexcitation, remain balanced over time owing to the Markovian processes.

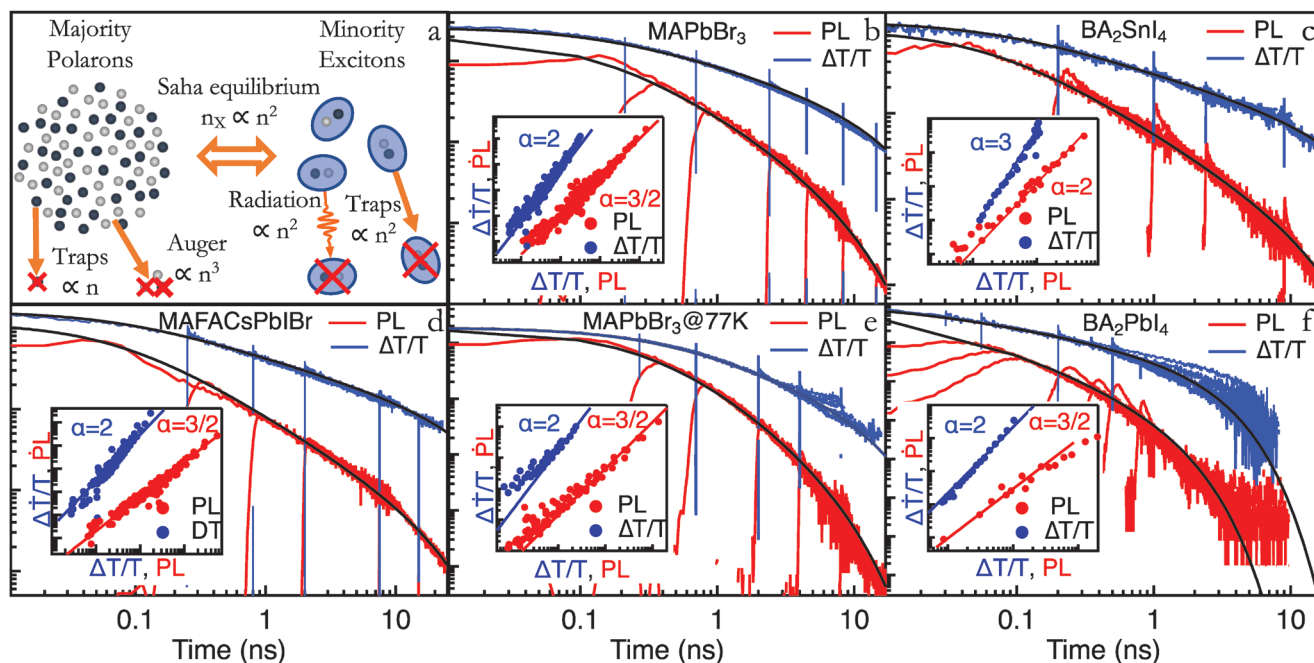


Figure 4. Markov dynamics of polaron and excitons according to rate equations. a) Sketch of the chemical equilibrium between a plasma of majority polarons and a minority population of bright excitons; decay channels are shown for both populations, but, because of the equilibrium, decay for each component also affects the other one. b–f) Series of differential transmission (blue lines) and photoluminescence (red lines) decays, each decay shifted in time according to the procedure discussed in the main text. The rate equation predictions are represented by the black lines; in each panel, the rate equation prediction for PL is the square of the rate equation prediction for differential transmission. The fact that a single rate equation curve can predict the whole dynamics of a series of time-shifted decays demonstrates the Markovian dynamics, that is, that the time evolution at time t only depends on the excited state density at time t and not on the density at previous times. In the insets, PL and DT time derivatives are plotted as a function of the PL and DT signal amplitudes; the slope in log-log scale represents therefore directly the order of the main decay channel in the rate equation.

Remarkably, Equations (1) and (2) are not a system of two independent equations, but effectively a single equation, due to the additional constraint that n_p and n_x are linked to each other ($n_p^2 = n_{eq} n_x$); there is therefore only one independent variable and the time decay of n_x is forced by the equilibrium condition to be always the square of the n_p decay. The rate equation to determine n_x is nonetheless explicitly reported to show how the kinetics of the minority species is affected by the interconversion rate establishing a quasi-stationary equilibrium state. In Equation (1), $k_{1,p}$ stems from polaron trapping. The third order term is proportional to $k_{3,p}$ and accounts for Auger recombination of three polarons. The second order constant $k_{2,p}$ is composed by two terms, $k_{r,p}$ representing the direct bimolecular radiative recombination of charged carriers, and $\frac{k_{1,x}}{n_{eq}}$, that comes from the monomolecular recombination of excitons and is a direct consequence of the chemical equilibrium regime, since decayed excitons need to be replenished from the polaron plasma. A decay driven by a quadratic term cannot be therefore taken as a proof of direct radiative recombination of unbound pairs. On the contrary, since PL spectra prove that light emission is excitonic in nature, the rate for direct emission from polarons $k_{r,p}$ can be neglected in HPs and hence $k_{2,p} \equiv \frac{k_{1,x}}{n_{eq}}$, a term that includes both the radiative and non-radiative monomolecular decay of excitons ($k_{1,x} = k_{r,x} + k_{nr,x}$). The equilibrium between polaron plasma and excitons provides therefore a natural explanation for the existence of a nonradiative bimolecular decay channel of polarons as the monomolecular decay of excitons mediated by the interconversion between excitons and polarons.

The rate equation for exciton population (Equation (2)) is very unconventional, since excitons are the minority species and their decay is entirely driven by the decay of the polaron density. The monomolecular decay of excitons is therefore due to polaron trapping, which just shows up in the exciton equation with a doubled rate. Exciton trapping, together with polaron bimolecular emission, comes back into the exciton rate equation as a term with exponent 3/2 that could never be produced with a single-species process and is therefore a distinctive feature of the equilibrium condition. The third term is also unexpected, as the quadratic term in the exciton rate equation is not due to bimolecular exciton-exciton annihilation,^[59] but is caused by Auger recombination of polarons followed by exciton-to-polaron conversion to maintain chemical equilibrium between the two species.

The functional dependence of PL and DT on the photoexcitation population put forward in the rate equations is fully confirmed by the experiments. Since PL monitors the exciton population ($PL(t) \propto n_x(t)$) and DT monitors polarons ($\frac{\Delta T}{T}(t) \propto n_p(t)$), our analysis protocol simply forecasts that the very same set of fit parameters ought to describe both PL and DT measurements. The pairs of black curves shown in each panel of Figure 4 represent coupled PL and DT decays obtained with the same parameters (reported in Table S2, Supporting Information); the agreement between experimental results and calculated curves encompasses four orders of magnitude in time, ranging from 1 ps to 20 ns.

Tandem spectroscopy measurements on different materials explore different regimes for the rate equations, confirming the existence of each of the unconventional terms. To avoid the pitfalls of a multi-parameter fit to the transient kinetics, which may not be very sensitive to the nature of the decay process, we directly identify the leading decay process by plotting in log scale (insets in Figure 4) the decay rates of PL and DT signals, \dot{PL} and $\frac{\Delta T}{T}$, that are proportional to the exciton and polaron populations, \dot{n}_x and \dot{n}_p , respectively, as a function of the signal amplitude themselves ($PL(t) \propto n_x(t)$ and $\frac{\Delta T}{T}(t) \propto n_p(t)$). In most cases, \dot{n}_p grows quadratically in n_p and \dot{n}_x increases as $n_x^{\frac{3}{2}}$, as predicted by the rate equations when the dominant decay channel is the monomolecular decay of excitons. The analysis for BA_2SnI_4 demonstrates the existence of cubic law in DT due to Auger recombination of polarons ($\dot{n}_p \propto n_p^3$) as leading decay rate, coupled to the quadratic term for excitons in PL.

3.3. Polaron Stabilization Energy

If polarons were the lowest-energy states, exciton radiative recombination would be thermally activated, in contrast with experimental evidences in $MAPbBr_3$ and $MAPbI_3$.^[61] Therefore, the polaron stabilization energy ($E_{p+} + E_{p-}$) is constrained to be lower than the exciton binding energy E_b . Reciprocity in presence of an exciton linewidth comparable to thermal energy $k_B T$ implies a Stokes shift ΔE_{PL} of the order of the linewidth itself, as the emitting states are the ones on the low-energy tail that are multiplied by a large Boltzmann factor, while the high-energy side of the exciton resonance is comparably suppressed. If we consider such redshift of the PL with respect to the exciton absorption peak, the constrain on polaron energy reads $E_{p+} + E_{p-} < E_b + \Delta E_{PL}$. In $MAPbBr_3$, $\Delta E_{PL} \approx 50$ meV and our experimental estimate of E_b was ≈ 60 meV,^[30] which leads to $E_{p+} + E_{p-} < 110$ meV; in $MAPbI_3$, the upper bound condition for the polaron energy is $E_{p+} + E_{p-} < 65$ meV ($\Delta E_{PL} \approx 40$ meV and $E_b \approx 25$ meV). Such values represent a rare experimental test for theoretical calculations of polaron energies, that have assessed $E_{p+} + E_{p-} \approx 70$ meV in $MAPbBr_3$ and ≈ 50 meV $MAPbI_3$.^[12,30] Several important questions are left to be explored, especially a precise determination of the polaron stabilization energy, understanding similarity and differences in polaron dynamics between 2D and 3D perovskites, how polaron-polaron interactions at high excitation fluences modify the stabilization energy and how stabilization energy is allocated to positive and negative polarons.

3.4. Comparison with Literature

The photophysics of HPs is the subject of a significant body of literature and it is important to establish how our experimental findings relate to published results. PL measurements taken on their own without the comparison to DT do not allow unambiguous identification of the excited-state species in 2D perovskites and the subsequent attribution of decay processes. The PL_0 dependence on laser fluence has been employed to identify the presence of free carriers in 3D perovskites,^[4,62,63]

but a superlinear PL_0 was reported also in 2D perovskites, consistent with our observation, although with a different interpretation.^[59]

DT measurements on 2D and 3D perovskites, without matching PL, can also be interpreted with the standard rate equation model, where nonlinear effects can be either attributed to carrier-carrier or exciton-exciton interactions; the DT portion of our measurements is therefore analogous to published results.^[6,55,64] The coexistence of bound excitons and large densities of polarons or free-carriers in MAPbBr₃ has been recently explored based on DT measurements.^[65] The assumption of polaron formation is also consistent with published results, since the sub-ps initial DT spectral dynamics as well as ultrafast coherent oscillations have been described as evidence for polaron formation, in agreement with our interpretation.^[11,17,66–68]

The most interesting comparison is perhaps with ultrafast measurements in the THz spectral region, where bound excitons and unbound carriers could be discriminated. THz measurements have provided, together with evidence for free carriers in 3D HPs and ultrafast exciton formation in 2D materials, some interesting signatures of significant presence of free carriers even in 2D perovskites and at low temperatures,^[38–42,66,67] where only excitons would have been expected. The overall scenario from THz measurements appears therefore compatible with our interpretation of contemporaneous presence of bright excitons and a polaron plasma.

While each piece of data we have presented is consistent with evidences presented in literature, the DT–PL comparison provided by the tandem spectroscopy technique allowed us to introduce the polaron-exciton dynamics to frame HP photo-physics, discussed in terms of a chemical thermodynamic equilibrium picture as guiding reference model.

4. Conclusions

Charged photoexcitations in hybrid metal HPs can form neutral exciton states with binding energies ranging from thermal energy, $k_B T$, up to several hundreds of meV. When the binding energy exceeds by far $k_B T$, for example, in 2D HPs or in 3D HPs at low enough temperature, excitons are expected to be the majority photoexcitation species, with significant implications for both charge transport and light emission properties. The light emission rate from a majority population of excitons is expected to scale linearly with the injected carrier density, radiative recombination of exciton being a monomolecular process. Yet, we have always observed a superlinear light emission rate, even at low temperature and in 2D HPs, an indication that a majority of excitons does not form. Measurements from a ultrafast tandem optical spectroscopy experiment, combining time-resolved PL and DT in a unified setup, allow to interpret such surprising result as the manifestation of a photoexcitation cycle characteristic of HP materials: a plasma of charged carriers- likely coupled to lattice deformation to form large polarons- forms in chemical quasi-equilibrium with a minority phase of excitons, even when the exciton binding energy by far exceeds thermal energy. Light emitted by HPs is resonant with the exciton transition, while its intensity is determined by

the concentration of non-emitting polarons, foreseeing novel mechanisms for LEDs and lasers. 2D HPs materials are considered more stable than 3D counterparts against degradation, but also less suitable for photovoltaics because insulating excitons were believed to prevent charge conduction in the excited state requiring significant energy loss for charge splitting. The presence of high concentrations of charged polarons in place of excitons suggests that such drawbacks are less serious than previously thought and provides a very positive outlook for efficient and stable photovoltaics employing layered perovskites.

5. Experimental Section

Materials Preparation: The 2D $n = 1$ perovskite films were fabricated by spin coating, at 3000 rpm for 30 s, a 0.13 M solution of 2D single crystals, synthesized as previously described,^[69] dissolved in anhydrous dimethylformamide (DMF) at 70 °C. After the deposition the films were annealed at 100 °C for 10 min.

The 2D $n = 1$ Sn perovskite films were prepared with $n\text{-CH}_3(\text{CH}_2)_3\text{NH}_2\text{I}$ (BAI) and SnI_2 dissolved in DMF with a molar ratio 2:1 and a final concentration of 0.5 M. The solution was pre-heated at 70 °C for 30 min then 50 μL were dropped on the substrate and spin-coated at 3000 rpm for 30 s. The film was annealed at 75 °C for 10 min.

The 3D Bromide and Iodide perovskite films were fabricated by one-pot and two-steps spin coating deposition, respectively. The $\text{CH}_3\text{NH}_3\text{PbBr}_3$ (MAPbBr₃) solution was prepared by dissolving MABr + $\text{PbAc}_2 \cdot 3\text{H}_2\text{O}$ with a molar ratio 3:1 in DMF and a final concentration of 0.5 M. The films were deposited on a glass slide at 6000 rpm for 60 s and then annealed at 100 °C for 5 min.

The $\text{CH}_3\text{NH}_3\text{PbI}_3$ (MAPbI₃) solution was prepared by dissolving MAI + PbCl_2 with a molar ratio 3:1 in DMF with a final concentration of 0.27 M. The solution was deposited on a glass slide at 6000 rpm then, after 6 s, 150 μL of chlorobenzene were dropped in the center of the spinning substrate and left to spin for an additional 30 s. A 100 °C thermal treatment was then performed for 50 min.

The $\text{MA}_{1-x-y}\text{FA}_x\text{Cs}_y\text{Pb}_{1-z}\text{Br}_z$ perovskite film was prepared with a 0.3 M precursor solution of FAI, MABr, CsI, PbI_2 , and PbBr_2 with final stoichiometry $\text{Cs}_{0.05}\text{FA}_{0.81}\text{MA}_{0.14}\text{Pb}_{1.55}\text{Br}_{0.45}$ in a mixed solvent of DMF and DMSO with a volume ratio of 4:1. The solution was deposited onto a glass substrate with a two-step spin coating procedure. First, two drops of solution were spun at 2000 rpm for 10 s with an acceleration of 200 rpm s^{-1} , then at 4000 rpm for 20 s with an acceleration of 1000 rpm s^{-1} . Ten seconds before the end of the whole spinning cycle, 100 μL of chlorobenzene were dropped on the substrate. The substrate was then thermally treated at 100 °C on a hotplate for 10 min.

All the film depositions were performed inside a nitrogen-filled glove box.

Materials Characterization: The X-ray diffraction patterns of the films were performed with a Siemens D5000 θ - 2θ diffractometer, with $\text{Cu } K_\alpha$ radiation and graphite monochromator. UV–vis optical absorption of HP films was measured with a dual-beam spectrophotometer equipped with an integrating sphere accessory (Agilent Technologies Cary 5000 UV–vis–NIR) to collect diffused transmission and reflection.^[70] A simpler procedure was employed only for BA_2SnI_4 , measuring just transmission in Perkin Elmer Lambda 950 dual beam spectrometer, in order to avoid sample degradation under ambient humidity.

Ultrafast Tandem Spectroscopy Setup: The laser source was a titanium:sapphire regenerative amplifier (Coherent Libra) delivering 100-fs long pulses, 794 nm in wavelength, up to 4 mJ in energy, with a 1 KHz repetition rate. The pump pulses were obtained with an optical parametric amplifier (Topas 800 from Light Conversion) equipped with nonlinear crystals. The DT spectrometer (Helios from Ultrafast Systems) measured individual probe and reference spectra with custom CMOS spectrometers achieving 1 nm spectral resolution. Home-made optomechanical modifications to the setup allowed collection

of luminescence, then dispersed with a grating spectrometer (Acton 2300i) and then detected with the streak camera (Hamamatsu C10910). The acquisition of PL and DT was done sequentially and the white light probe was blocked while measuring PL. BA₂SnI₄ films were kept in vacuum during measurements.

Physical Origin of the DT Signal: A DT signal at the lowest allowed exciton resonance (X_0 , namely the one observed in PL) can be due to phase space filling, collisional broadening and other nonlinear interactions. None of these mechanisms necessarily requires a population of the bright excitons X_0 . A vast body of work has addressed such topic, both experimentally and theoretically, in inorganic semiconductors with delocalized electronic states (in particular, see the fundamental work by Schmitt-Rink and coworkers in the 80s).^[7] As an example, nonlinear interactions of the excitons X_0 with a majority population of dark states can lead to a renormalization of the X_0 wavefunction, which in turns modifies the oscillator strength. The resulting DT signal at the X_0 resonance is proportional to the majority population of dark states. Bleaching of the X_0 transition induced by phase space filling was addressed as follows. The exciton state is a composite particle made by a pair of interacting electrons and holes. According to Schmitt-Rink et al.'s theory, an exciton cannot be created in regions of the semiconductor where another electron (or hole, or both) is present because of the Pauli's exclusion principle. As a consequence, the DT signal induced at the X_0 transition is proportional to the sum $an_e + bn_h$, where a and b are constants, while n_e and n_h are, respectively, the overall populations of the electrons and holes. It is worth pointing out that exciton bleaching cannot be ascribed to ground state bleach alone, but includes the excited state, as both ground and excited states may be partly occupied by free carriers, or shared by composite multiparticle states such as excitons, trions, biexcitons, trap states, and so on. The bleaching electrons, or holes, can therefore be part of another bound or unbound electron-hole state, that can be either dark or bright, and may not necessarily coincide with the X_0 exciton on which bleaching is detected. As an example, the case of a bleaching quasi two-particle state made by an unbound electron and hole pair could be considered, the former with wavevector $k = 0$ and the second with wavevector much larger than the inverse of the X_0 radius. This state is dark (direct one-photon transition was forbidden), but the electron (not the hole) contributes to the bleaching of the X_0 transition. Even more illuminating was the case of an X_0 exciton with wavevector smaller than the inverse of the exciton radius, but not null. As only X_0 excitons with $k \approx 0$ are bright, this bound electron-hole state is dark, but, as in the previous case, provides a not negligible contribution to bleaching of the X_0 transition. Same reasoning applies to electrons and holes that, because of lattice relaxation, form large polaron states. Finally, it is worth pointing out that all these bleaching mechanisms scale linearly with the population of the majority species for not too large excitation densities.

Markov Plots and Rate Equations: Whether or not the photoexcitation kinetics can be described as a Markovian process depends on several factors: intrinsic and extrinsic properties of the materials, the excitation regime and so on. For this reason, Markovian plots were exploited as a general and powerful tool to demonstrate basic properties of the excited-states in hybrid perovskites, as discussed below, which could not be unambiguously demonstrated by passing through complicated, and often controversial, multiparameter fit analyses.

The kinetics of charged and neutral photoexcitations would imply considering at least six unknown quantities, the population of free and trapped positive and negative charge carriers, and the population of free and trapped excitons. The Markovian plots for both the DT and PL transients demonstrated unequivocally that the total excitation density was sole independent variable determining the overall kinetics of excitons and charged carriers. How could this happen in a complex dynamic system in which six populations evolved according to six coupled first order ordinary equations (ODEs)? Three are the basic conditions that allow the excited-state transients to be described as a Markovian process: i) the excited species leading to the DT signal (namely, the majority population of charged carriers) and that responsible for the PL (namely, the minority population of excitons) reach the thermodynamic

equilibrium in a short time so that at any instant following excitation the population of one species determines the population of the other one; ii) The populations of trapped particles do not play a role in the DT and PL transients in the investigated time-scales, and therefore can be neglected in the coupled ODEs. This does not mean that excitons and charged carriers are not trapped somewhere in the surface or the bulk of the crystal, as they actually are: it simply states that trapping processes enter the ODEs of exciton and charged carrier populations only through constant terms (i.e., which do not depend neither on time nor on space) and do not depend on trap populations (i.e., the rate equations for exciton and charged carrier populations are not coupled to the ODEs describing the population of trap states). If this were not the case, the solution of the ODE systems of excitons and charged particles would depend on the degree of trap filling, which is determined by the previous history of the relaxation process (and not just by the overall carrier population), and hence the photoexcitation kinetics could not be described as a Markovian process; iii) The population of positive and negative charged carriers are equal. If this condition were not satisfied, the populations of opposite charged carriers would again depend on previous times of the relaxation process and not just on the overall carrier population at a given instant.

Derivation of the Rate Equations for Polaron and Exciton Populations: The time derivatives \dot{n}_p and \dot{n}_x for polaron and exciton populations, once the generation with the pulsed laser was over, can be written accounting for a monomolecular, quadratic and Auger decay for polarons (with constants $k_{1,p}$, $k_{r,p}$ and $k_{3,p}$ respectively, where the r subscript in the quadratic term stands for radiative), as well as a monomolecular decay term for excitons (proportional to $k_{1,x}$) and an equilibration term that converts excitons into polarons and vice versa driving populations toward chemical equilibrium:

$$\dot{n}_p \equiv -k_{1,p}n_p^2 - k_{r,p}n_p^2 - k_{3,p}n_p^3 - C\left(\frac{n_p^2}{n_{eq}} - n_x\right) \quad (3)$$

$$\dot{n}_x \equiv -k_{1,x}n_x + C\left(\frac{n_p^2}{n_{eq}} - n_x\right) \quad (4)$$

The total population $n = n_p + n_x$ would then decay with the sum of the two rates:

$$\dot{n} \equiv -k_{1,p}n_p - k_{r,p}n_p^2 - k_{3,p}n_p^3 - k_{1,x}n_x \quad (5)$$

Assuming the equilibrium is always maintained, the additional condition $n_p^2 = n_{eq}n_x$ has to be met.

Furthermore, experiments demonstrated that polarons are the majority species, so that their decay rate would be well approximated by the total rate:

$$\dot{n}_p \equiv \dot{n} \equiv -k_{1,p}n_p - \left(k_{r,p} + \frac{k_{1,x}}{n_{eq}}\right)n_p^2 - k_{3,p}n_p^3 \quad (6)$$

meaning that because of the equilibrium condition, the decay of excitons showed up as a quadratic decay term in the population of polarons, since polarons were depleted to replenish the decayed excitons.

Since exciton and polaron populations were linked by their equilibrium conditions, so were their decay rates, as obtained by taking the time derivative of chemical equilibrium: $2n_p\dot{n}_p = n_{eq}\dot{n}_x$.

This was the reason why decays of order α for polarons, that is, proportional to n_p^α , produce terms $\propto n_p^{\alpha+1} \propto n_x^{\frac{\alpha+1}{2}}$ in the exciton decay rate.

Now \dot{n}_x can be simply obtained as:

$$\begin{aligned} \dot{n}_x &= \frac{2n_p\dot{n}_p}{n_{eq}} \equiv -2k_{1,p}\frac{n_p^2}{n_{eq}} - 2\left(k_{r,p} + \frac{k_{1,x}}{n_{eq}}\right)\frac{n_p^3}{n_{eq}} \\ &- 2k_{3,p}\frac{n_p^4}{n_{eq}} = -2k_{1,p}n_x - 2\left(k_{r,p} + \frac{k_{1,x}}{n_{eq}}\right)n_{eq}^{\frac{1}{2}}\frac{n_x^{\frac{3}{2}}}{n_x^{\frac{1}{2}}} - 2k_{3,p}n_{eq}n_x^2 \end{aligned} \quad (7)$$

Since the density of excitons appear always to much lower than polaron density, exciton–exciton interaction has not been included for consistency, as it would produce a term proportional to n_p^4 in the rate equation for polarons and to n_X^2 in the rate equation for excitons.

The Modified Saha Equation for Polaron and Exciton Populations: The populations of excitons and polarons can be expressed in terms of their chemical potentials (μ_X, μ_{p+} , and μ_{p-} for excitons, positive, and negative polarons, respectively) as follows:

$$n_X = 4 \left[\frac{k_B T (m_e + m_h)}{2\pi\hbar^2} \right]^3 e^{-\frac{E_g - E_c - E_v - \mu_X}{k_B T}} \quad (8)$$

$$n_{p-} = 2 \left(\frac{k_B T m_{p-}}{2\pi\hbar^2} \right)^3 e^{-\frac{E_c - E_{p-} - \mu_{p-}}{k_B T}} \quad (9)$$

$$n_{p+} = 2 \left(\frac{k_B T m_{p+}}{2\pi\hbar^2} \right)^3 e^{-\frac{E_v + E_{p+} - \mu_{p+}}{k_B T}} \quad (10)$$

where E_g is the energy gap; E_c and E_v are the energies of the conduction and valence band extrema, respectively. If polarons are in chemical equilibrium with excitons, it follows that the chemical potentials of polarons pairs and that of excitons are equal: $\mu_{p+} + \mu_{p-} = \mu_X$. The modified Saha equation thus reads:

$$\frac{n_{p+} n_{p-}}{n_X} = n_{eq} = \left(\frac{k_B T \tilde{m}_p}{2\pi\hbar^2} \right)^3 e^{-\frac{E_c - (E_{p+} + E_{p-})}{k_B T}} \quad (11)$$

where $\tilde{m}_p = \frac{m_{p+} m_{p-}}{m_e + m_h}$. In the limit of a negligible polaron effect ($E_{p+} + E_{p-} \rightarrow 0$, $m_{p-(+)} \rightarrow m_{e(h)}$), the usual Saha equation is recovered.

Analysis of DT for Polaron Formation and Size: The sub-picosecond DT transients were analyzed in analogy to reports in literature that have attributed such transients to polaron formation.^[11,23] The results of MAPbBr₃ and BA₂SnI₄, representative of 3D and 2D HPs, respectively were discussed. Figure S8, Supporting Information shows the initial decay of the DT signal, for photon energies close to the exciton resonance for different pulse fluences. The fast contribution vanished at the highest excitations. However, as shown, this behavior did not monitor the inhibition of polaron formation at high densities, but rather a modification of many-body interactions when polaron states are not formed yet. DT spectra acquired at two delays are reported in Figure S8, Supporting Information: the first one was taken at the maximum of the spikes reported in Figure 4, $t_1 = 0.3$ ps, at the early stage of lattice relaxation, which was expected to be completed within 1 ps;^[11] the second one at $t_2 = 2$ –5 ps, when the fast contribution had disappeared and photoexcitations were dressed by lattice distortion. The quantity of interest here is the change in absorbance induced by polaron formation. These perturbations can be monitored by analyzing the difference between DT spectra taken at the two delays, t_1 and t_2 . For MAPbBr₃ at 77 K (Figure S8A, Supporting Information) at low pulse fluences ($\varphi = 1 \mu\text{cm}^{-2}$), the difference spectrum presents a negative peak centred at the exciton resonance, corresponding to a bleaching of the excitonic transition, counterbalanced by an induced absorption of equal strength on the low energy side. The nonlinear absorption signal to the excitation of a trion state, namely a composite particle made by an electron (hole) bound to an exciton was attributed. The photon absorption cross-section to form the three-particle state in presence of a population of charged carriers (electrons or holes) occurred at the expense of the optical excitation of neutral excitons, thus leading to a comparable reduction of the exciton oscillator strength. After reorganization of the polar lattice around charged carriers, Coulomb screening was enhanced, making the trion state unstable and, consequently, inducing the disappearance of the associated absorption peak and an increase of

absorption at the exciton resonance. Increasing fluences, the difference spectrum broadened and the zero crossing shifted to higher energies until it matches the exciton energy. The observed spectral shape now monitored a red shift of the exciton line produced by the initially photoexcited electron–hole plasma. At these fluences, the higher plasma density screened the Coulomb interaction between excitons and free carriers, which on one side destabilized trion states but, on the other hand, induced a redshift of the exciton resonance. Both this latter many-body effect and the trion resonance gradually disappeared after polaron formation. The sub-picosecond transient of the nonlinear response, triggered by lattice relaxation in the excited-state, was observed even at the highest fluences, $\varphi = 36 \mu\text{J cm}^{-2}$, corresponding to an injected photoexcitation population of $5.7 \times 10^{18} \text{ cm}^{-3}$, equivalent to a polaron–polaron mean distance $r = 6.9$ nm (see Figure S8, Supporting Information). Polar lattice deformations around the electronic excitations have a finite extension r_p . At high excitations, the interparticle distance could approach $2r_p$. Polaron–polaron interaction was expected to trigger a readjustment of the phonon cloud around charged carriers, which would result in polaron states with a more free-carrier character. In the low-density limit, first-principle calculations provided a lower bound estimate for positive polarons in MAPbBr₃, $2r_p = 5.0$ nm, which was smaller than the minimum interparticle distance reached in the highest excitation regime investigated in the experiments.^[12,14,24,30] It was finally recalled that the excitonic resonance was still well resolved even at the highest fluences, which meant that the excited semiconductor was well below the Mott density above which bound electron–hole states could not exist. Figure S8, Supporting Information also shows the nonlinear response of BA₂SnI₄. With respect to the case of MAPbBr₃, only the low-density regime in which optical formation of trions was inhibited after lattice reorganization around charged carriers was observed. Finally, ultrafast transients lasted a few hundred femtoseconds as in MAPbBr₃, with an intensity that was independent of fluence.

Supporting Information

Supporting Information is available from the Wiley Online Library or from the author.

Acknowledgements

A.S. and R.P. contributed equally to this work. The authors acknowledge access to research infrastructure in CeSAR—Centro Servizi di Ateneo per la Ricerca—at the Università degli Studi di Cagliari and thank Dr. M. Marceddu for technical assistance. This work was funded by Regione Autonoma della Sardegna through PO-FSE Sardegna 2007–2013, L.R. 7/2007, “Progetti di ricerca di base e orientata,” Projects Nos. CRP3-114, CRP-17571, CRP-18353, CRP- 18013, and CRP-24978, and through Delibera CIPE n. 31 del 20.02.2015 e deliberazione n. 52/36 del 28.10.2015 “Piano Strategico Sulcis,” through Project Nos. SULCIS-820889 and SULCIS-820947, as well as by MIUR (Italian Ministry of University and Research) through PRIN PERovskite-based solar cells: toward high efficiency and long-term stability (PERSEO), project id 20155LECAJ. The work was also supported by Fondazione di Sardegna through project 2F20000210007 “Perovskite materials for photovoltaics.” A.S. was supported by PON “Ricerca e Innovazione” 2014–2020—Fondo sociale europeo, Attraction and International Mobility—Codice AIM1809115 Num. Attività 2, Linea 2.1. Work at Northwestern was supported by the US Department of Energy, Office of Science, Basic Energy Sciences, under Grant No. SC0012541 (sample synthesis, measurements, and characterization).

Conflict of Interest

The authors declare no conflict of interest.

Data Availability Statement

The data that support the findings of this study are available from the corresponding author upon reasonable request.

Keywords

2D perovskites, excitons, hybrid perovskites, polarons, ultrafast spectroscopy

Received: February 17, 2021

Revised: April 13, 2021

Published online:

- [1] C. C. Stoumpos, M. G. Kanatzidis, *Acc. Chem. Res.* **2015**, *48*, 2791.
- [2] L. M. Herz, *Annu. Rev. Phys. Chem.* **2016**, *67*, 65.
- [3] J. Huang, Y. Yuan, Y. Shao, Y. Yan, *Nat. Rev. Mater.* **2017**, *2*, 17042.
- [4] M. Saba, M. Cadelano, D. Marongiu, F. Chen, V. Sarritzu, N. Sestu, C. Figus, M. Aresti, R. Piras, A. Geddo Lehmann, C. Cannas, A. Musinu, F. Quochi, A. Mura, G. Bongiovanni, *Nat. Commun.* **2014**, *5*, 5049.
- [5] V. D'Innocenzo, G. Grancini, M. J. P. Alcocer, A. R. S. Kandada, S. D. Stranks, M. M. Lee, G. Lanzani, H. J. Snaith, A. Petrozza, *Nat. Commun.* **2014**, *5*, 3586.
- [6] J. S. Manser, P. V. Kamat, *Nat. Photonics* **2014**, *8*, 737.
- [7] D. Marongiu, M. Saba, F. Quochi, A. Mura, G. Bongiovanni, *J. Mater. Chem. C* **2019**, *7*, 12006.
- [8] C. C. Stoumpos, D. H. Cao, D. J. Clark, J. Young, J. M. Rondinelli, J. I. Jang, J. T. Hupp, M. G. Kanatzidis, *Chem. Mater.* **2016**, *28*, 2852.
- [9] T. M. Koh, B. Febriansyah, N. Mathews, *Chem* **2017**, *2*, 326.
- [10] H. Tsai, W. Nie, J. C. Blancon, C. C. Stoumpos, R. Asadpour, B. Harutyunyan, A. J. Neukirch, R. Verduzco, J. J. Crochet, S. Tretiak, L. Pedesseau, J. Even, M. A. Alam, G. Gupta, J. Lou, P. M. Ajayan, M. J. Bedzyk, M. G. Kanatzidis, A. D. Mohite, *Nature* **2016**, *536*, 312.
- [11] G. Batignani, G. Fumero, A. R. Srimath Kandada, G. Cerullo, M. Gandini, C. Ferrante, A. Petrozza, T. Scopigno, *Nat. Commun.* **2018**, *9*, 1971.
- [12] D. Ghosh, E. Welch, A. J. Neukirch, A. Zakhidov, S. Tretiak, *J. Phys. Chem. Lett.* **2020**, *11*, 3271.
- [13] H. Cho, Y. H. Kim, C. Wolf, H. D. Lee, T. W. Lee, *Adv. Mater.* **2018**, *30*, 1704587.
- [14] C. Motta, S. Sanvito, *J. Phys. Chem. C* **2018**, *122*, 1361.
- [15] T. Ivanovska, C. Dionigi, E. Mosconi, F. De Angelis, F. Liscio, V. Morandi, G. Ruani, *J. Phys. Chem. Lett.* **2017**, *8*, 3081.
- [16] M. Schlipf, S. Ponc e, F. Giustino, *Phys. Rev. Lett.* **2018**, *121*, 086402.
- [17] H. Zhu, K. Miyata, Y. Fu, J. Wang, P. P. Joshi, D. Niesner, K. W. Williams, S. Jin, X. Y. Zhu, *Science* **2016**, *353*, 1409.
- [18] F. G. Santomauro, J. Grilj, L. Mewes, G. Nedelcu, S. Yakunin, T. Rossi, G. Capano, A. Al Haddad, J. Budarz, D. Kinschel, D. S. Ferreira, G. Rossi, M. G. Tovar, D. Grolimund, V. Samson, M. Nachttegaal, G. Smolentsev, M. V. Kovalenko, M. Chergui, *Struct. Dyn.* **2017**, *4*, 044002.
- [19] C. Liu, H. Tsai, W. Nie, D. J. Gosztola, X. Zhang, *J. Phys. Chem. Lett.* **2020**, *11*, 6256.
- [20] M. Puppini, S. Polishchuk, N. Colonna, A. Crepaldi, D. N. Dirin, O. Nazarenko, R. De Gennaro, G. Gatti, S. Roth, T. Barillot, L. Poletto, R. P. Xian, L. Rettig, M. Wolf, R. Ernstorfer, M. V. Kovalenko, N. Marzari, M. Grioni, M. Chergui, *Phys. Rev. Lett.* **2019**, *124*, 206402.
- [21] J. M. Frost, L. D. Whalley, A. Walsh, *ACS Energy Lett.* **2017**, *2*, 2647.
- [22] D. Niesner, H. Zhu, K. Miyata, P. P. Joshi, T. J. S. Evans, B. J. Kudisch, M. T. Trinh, M. Marks, X. Y. Zhu, *J. Am. Chem. Soc.* **2016**, *138*, 15717.
- [23] K. Miyata, D. Meggiolaro, M. T. Trinh, P. P. Joshi, E. Mosconi, S. C. Jones, F. De Angelis, X. Y. Zhu, *Sci. Adv.* **2017**, *3*, e1701217.
- [24] M. Bokdam, T. Sander, A. Stroppa, S. Picozzi, D. D. Sarma, C. Franchini, G. Kresse, *Sci. Rep.* **2016**, *6*, 28618.
- [25] F. Zheng, L. W. Wang, *Energy Environ. Sci.* **2019**, *12*, 1219.
- [26] H. H. Fang, S. Adjokatse, S. Shao, J. Even, M. A. Loi, *Nat. Commun.* **2018**, *9*, 243.
- [27] S. Kahmann, M. A. Loi, *J. Mater. Chem. C* **2019**, *7*, 2471.
- [28] M. Li, J. Fu, Q. Xu, T. C. Sum, *Adv. Mater.* **2019**, *31*, 1802486.
- [29] J. M. Frost, *Phys. Rev. B* **2017**, *96*, 195202.
- [30] D. Meggiolaro, F. Ambrosio, E. Mosconi, A. Mahata, F. De Angelis, *Adv. Energy Mater.* **2019**, *10*, 1902748.
- [31] A. Mahata, D. Meggiolaro, F. De Angelis, *J. Phys. Chem. Lett.* **2019**, *10*, 1790.
- [32] A. M. Soufiani, F. Huang, P. Reece, R. Sheng, A. Ho-Baillie, M. A. Green, *Appl. Phys. Lett.* **2015**, *107*, 231902.
- [33] J. Yin, P. Maity, R. Naphade, B. Cheng, J. H. He, O. M. Bakr, J. L. Br edas, O. F. Mohammed, *ACS Nano* **2019**, *13*, 12621.
- [34] A. R. Srimath Kandada, C. Silva, *J. Phys. Chem. Lett.* **2020**, *11*, 3173.
- [35] H. Esmaielpour, V. R. Whiteside, S. Sourabh, G. E. Eperon, J. T. Pecht, M. C. Beard, H. Lu, B. K. Durant, I. R. Sellers, *J. Phys. Chem. C* **2020**, *124*, 9496.
- [36] J. Yin, H. Li, D. Cortecchia, C. Soci, J. L. Br edas, *ACS Energy Lett.* **2017**, *2*, 417.
- [37] X. Jia, J. Jiang, Y. Zhang, J. Qiu, S. Wang, Z. Chen, N. Yuan, J. Ding, *Appl. Phys. Lett.* **2018**, *112*, 143903.
- [38] M. C. G elvez-Rueda, E. M. Hutter, D. H. Cao, N. Renaud, C. C. Stoumpos, J. T. Hupp, T. J. Savenije, M. G. Kanatzidis, F. C. Grozema, *J. Phys. Chem. C* **2017**, *121*, 26566.
- [39] A. Kumar, A. Solanki, M. Manjappa, S. Ramesh, Y. K. Srivastava, P. Agarwal, T. C. Sum, R. Singh, *Sci. Adv.* **2020**, *6*, eaax8821.
- [40] G. Folpini, L. Gatto, D. Cortecchia, M. Devetta, G. Crippa, C. Vozzi, S. Stagira, A. Petrozza, E. Cinquanta, *J. Chem. Phys.* **2020**, *152*, 214705.
- [41] O. F. Williams, N. Zhou, J. Hu, Z. Ouyang, A. Kumbhar, W. You, A. M. Moran, *J. Phys. Chem. A* **2019**, *123*, 11012.
- [42] A. Burgos-Caminal, E. Socie, M. E. F. Bouduban, J. E. Moser, *J. Phys. Chem. Lett.* **2020**, *11*, 7692.
- [43] L. Luo, L. Men, Z. Liu, Y. Mudryk, X. Zhao, Y. Yao, J. M. Park, R. Shinar, J. Shinar, K. M. Ho, I. E. Perakis, J. Vela, J. Wang, *Nat. Commun.* **2017**, *8*, 15565.
- [44] F. Deschler, M. Price, S. Pathak, L. E. Klintberg, D. D. Jarausch, R. Higler, S. H uttner, T. Leijtens, S. D. Stranks, H. J. Snaith, M. Atat ure, R. T. Phillips, R. H. Friend, *J. Phys. Chem. Lett.* **2014**, *5*, 1421.
- [45] J.-P. Correa-Baena, M. Saliba, T. Buonassisi, M. Gr atzel, A. Abate, W. Tress, A. Hagfeldt, *Science* **2017**, *358*, 739.
- [46] M. Wei, K. Xiao, G. Walters, R. Lin, Y. Zhao, M. I. Saidaminov, P. Todorovi c, A. Johnston, Z. Huang, H. Chen, A. Li, J. Zhu, Z. Yang, Y. K. Wang, A. H. Proppe, S. O. Kelley, Y. Hou, O. Voznyy, H. Tan, E. H. Sargent, *Adv. Mater.* **2020**, *32*, 1907058.
- [47] W. Ke, C. C. Stoumpos, M. Zhu, L. Mao, I. Spanopoulos, J. Liu, O. Y. Kontsevoi, M. Chen, D. Sarma, Y. Zhang, M. R. Wasielewski, M. G. Kanatzidis, *Sci. Adv.* **2017**, *3*, e1701293.
- [48] M. Baranowski, P. Plochocka, *Adv. Energy Mater.* **2020**, *10*, 1903659.
- [49] Y. Jiang, X. Wang, A. Pan, *Adv. Mater.* **2019**, *31*, 1806671.
- [50] N. Sestu, M. Cadelano, V. Sarritzu, F. Chen, D. Marongiu, R. Piras, M. Mainas, F. Quochi, M. Saba, A. Mura, G. Bongiovanni, *J. Phys. Chem. Lett.* **2015**, *6*, 4566.
- [51] C. L. Davies, M. R. Filip, J. B. Patel, T. W. Crothers, C. Verdi, A. D. Wright, R. L. Milot, F. Giustino, M. B. Johnston, L. M. Herz, *Nat. Commun.* **2018**, *9*, 293.

- [52] V. Sarritzu, N. Sestu, D. Marongiu, X. Chang, S. Masi, A. Rizzo, S. Colella, F. Quochi, M. Saba, A. Mura, G. Bongiovanni, *Sci. Rep.* **2017**, *7*, 44629.
- [53] M. Stolterfoht, C. M. Wolff, J. A. Márquez, S. Zhang, C. J. Hages, D. Rothhardt, S. Albrecht, P. L. Burn, P. Meredith, T. Unold, D. Neher, *Nat. Energy* **2018**, *3*, 847.
- [54] B. Anand, S. Sampat, E. O. Danilov, W. Peng, S. M. Rupich, Y. J. Chabal, Y. N. Gartstein, A. V. Malko, *Phys. Rev. B* **2016**, *93*, 161205.
- [55] Y. Yang, M. Yang, Z. Li, R. Crisp, K. Zhu, M. C. Beard, *J. Phys. Chem. Lett.* **2015**, *6*, 4688.
- [56] K. Pydzińska, J. Karolczak, M. Szafranski, M. Ziótek, *RSC Adv.* **2018**, *8*, 6479.
- [57] J. M. Ball, A. Petrozza, *Nat. Energy* **2016**, *1*, 16149.
- [58] V. Sarritzu, N. Sestu, D. Marongiu, X. Chang, Q. Wang, M. A. Loi, F. Quochi, M. Saba, A. Mura, G. Bongiovanni, *Adv. Opt. Mater.* **2018**, *6*, 1700839.
- [59] G. Delport, G. Chehade, F. Lédeé, H. Diab, C. Milesi-Brault, G. Trippé-Allard, J. Even, J. S. Lauret, E. Deleporte, D. Garrot, *J. Phys. Chem. Lett.* **2019**, *10*, 5153.
- [60] J. M. Richter, M. Abdi-Jalebi, A. Sadhanala, M. Tabachnyk, J. P. H. Rivett, L. M. Pazos-Outón, K. C. Gödel, M. Price, F. Deschler, R. H. Friend, *Nat. Commun.* **2016**, *7*, 13941.
- [61] V. Sarritzu, N. Sestu, D. Marongiu, X. Chang, Q. Wang, S. Masi, S. Colella, A. Rizzo, A. Gocalinska, E. Pelucchi, M. L. Mercuri, F. Quochi, M. Saba, A. Mura, G. Bongiovanni, *Adv. Opt. Mater.* **2018**, *6*, 1701254.
- [62] M. B. Johnston, L. M. Herz, *Acc. Chem. Res.* **2016**, *49*, 146.
- [63] M. Saba, F. Quochi, A. Mura, G. Bongiovanni, *Acc. Chem. Res.* **2016**, *49*, 166.
- [64] J. Cho, J. T. DuBose, P. V. Kamat, *J. Phys. Chem. Lett.* **2020**, *11*, 2570.
- [65] T. Palmieri, E. Baldini, A. Steinhoff, A. Akrap, M. Kollár, E. Horváth, L. Forró, F. Jahnke, M. Chergui, *Nat. Commun.* **2020**, *11*, 850.
- [66] T. Ghosh, S. Aharon, L. Etgar, S. Ruhman, *J. Am. Chem. Soc.* **2017**, *139*, 18262.
- [67] W. Zhao, Z. Qin, C. Zhang, G. Wang, X. Dai, M. Xiao, *Appl. Phys. Lett.* **2019**, *115*, 243101.
- [68] Z. Liu, C. Vaswani, L. Luo, D. Cheng, X. Yang, X. Zhao, Y. Yao, Z. Song, R. Brenes, R. J. H. Kim, J. Jean, V. Bulović, Y. Yan, K.-M. Ho, J. Wang, *Phys. Rev. B* **2020**, *101*, 115125.
- [69] D. H. Cao, C. C. Stoumpos, O. K. Farha, J. T. Hupp, M. G. Kanatzidis, *J. Am. Chem. Soc.* **2015**, *137*, 7843.
- [70] D. Marongiu, S. Lai, V. Sarritzu, E. Pinna, G. Mula, M. Laura Mercuri, M. Saba, F. Quochi, A. Mura, G. Bongiovanni, M. L. M. L. Mercuri, M. Saba, F. Quochi, A. Mura, G. Bongiovanni, *ACS Appl. Mater. Interfaces* **2019**, *11*, 10021.
- [71] S. Schmitt-Rink, D. S. Chemla, D. A. B. Miller, *Phys. Rev. B* **1985**, *32*, 6601.